Unexpected dissemination patterns in lymphoma progression revealed by serial imaging within a murine lymph node

Ken Ito[1,2,*], **Bryan Ronain Smith**[1,2,*], **Natesh Parashurama**[1,2], **Joon-Kee Yoon**[1,2,3], **Si Yeol Song**[1,2,4], **Cornelius Miething**[5], **Parag Mallick**[1,2], **Scott Lowe**[5], and **Sanjiv Sam Gambhir**[1,2]

[1]Molecular Imaging Program at Stanford, Stanford University

[2]Department of Radiology, Stanford University

[3]Department of nuclear medicine & molecular imaging, Ajou University School of Medicine, Suwon, Korea

[4]Department of Radiation Oncology, University of Ulsan College of Medicine, Seoul, Korea

[5]Cold Spring Harbor Laboratories

Abstract

Non-Hodgkin's lymphoma (NHL) is a heterogeneous and highly disseminated disease, but the mechanisms of its growth and dissemination are not well understood. Using a mouse model of this disease, we employed multimodal imaging, including intravital microscopy (IVM) combined with bioluminescence, as a powerful tool to better elucidate NHL progression. We injected EGFP and luciferase-expressing Eμ-Myc/Arf–/– (Cdkn2a–/–) mouse lymphoma cells (EL-Arf–/–) into C57BL/6NCrl mice intravenously. Long-term observation inside a peripheral lymph node was enabled by a novel lymph node internal window chamber (LNIWC) technique that allows chronic, sequential lymph node imaging under in vivo physiological conditions. Interestingly, during early stages of tumor progression we found that few if any lymphoma cells homed initially to the inguinal lymph node, despite clear evidence of lymphoma cells in the bone marrow and spleen. Unexpectedly, we detected a reproducible efflux of lymphoma cells from spleen and bone marrow, concomitant with a massive and synchronous influx of lymphoma cells into the inguinal lymph node, several days after injection. We confirmed a coordinated efflux/influx of tumor cells by injecting EL-Arf–/– lymphoma cells directly into the spleen and observing a burst of lymphoma cells, validating that the burst originated in organs remote from the lymph nodes. Our findings argue that in NHL an efflux of tumor cells from one disease site to another, distant site where they become established occurs in discrete bursts.

Keywords

Introduction

Human Non-Hodgkin's Lymphoma (NHL) is a heterogeneous and highly disseminated disease that includes very aggressive subtypes which display explosive growth, such as Burkitt's lymphoma(1). The mechanisms and microscale details of lymphoma growth and dissemination are not yet well-understood. Yet such knowledge could greatly improve strategies for early detection and management of lymphoma patients. Reliable approaches for longitudinal monitoring of lymph nodes in animal models are thus critical to help elucidate biological phenomena occurring in lymph nodes.

To directly address the mechanisms of lymphoma progression, we focused on the murine inguinal lymph node and imaged cancer progression using intravital microscopy (IVM) combined with bioluminescence imaging in living mice. We employed the *Eμ-myc* transgenic mouse model, which expresses the *Myc* oncogene in the B cell compartment, resulting in mice with transplantable lymphomas. This orthotopic mouse lymphoma model was chosen because it captures critical genetic and pathological features of the human disease (2, 3). IVM has long been a useful tool to address unknown biological mechanisms in diverse fields including immunology(4-6), cancer biology(7-11), nanoparticle delivery(12-14), drug discovery(15) and biomarker research(16), etc in animal models. Though lymph nodes have been imaged in mice using IVM for over a decade(17, 18), current techniques to directly and chronically image a lymph node microscopically are still lacking. Because of the lack of a chronic microscale lymph node imaging technique reported in the literature, we established one for the serial visualization of lymphoma development under physiological conditionsand combined it with bioluminescence imaging in order to reveal the mechanisms by which lymphoma actually forms.

Normal lymphocyte trafficking is essential for the regulation of systemic immune processes, as well as lymphocyte differentiation and development. Most mature lymphocytes recirculate continuously from blood to tissue and back to the blood again(19). This recirculation is regulated by lymphocyte-endothelial interactions mediated by adhesion molecules (e.g., L-selectin, CD44, integrin, VLA-4, and LFA-1) and select chemokines(20, 21). Such interactions may be maintained in lymphoma trafficking patterns; it is believed that unlike the metastasis of other cancers, lymphoma dissemination likely reflects conserved physiologic behavior - normal lymphocyte homing and recirculation molecules have been implicated in lymphoma dissemination and invasion(20, 21). However, the precise mechanisms and time frame of lymphoma trafficking are not well-understood. Improved methods and targets for detection and therapy of the disease could likely result from understanding the time course and mechanisms(20, 21), particularly unpredictable characteristics of disease that diverge from normal trafficking patterns.

In this study, we developed a novel lymph node internal window chamber (LNIWC) and with bioluminescence examined lymphoma growth and dissemination in spatial and temporal detail. We made surprising observations that appear to constitute processes distinct from normal lymphocyte homing patterns: for instance, within a 12 hour period identified via chronic serial imaging, we reproducibly observed a large, rapid efflux from the bone marrow and spleen, with a concomitant influx of lymphoma cells into the inguinal lymph node (ILN) region.

Materials and Methods

Cell culture

Eμ-myc/Arf−/− lymphoma cells which harbor loss-of-function regions in the *Arf gene* were derived by intercrossing *Eμ-myc* transgenic mice with *Arf*-null mice, all in the C57BL/6

background as described previously(2). *Eμ-myc/Arf–/–* Lymphoma cells and EL-Arf–/– lymphoma cells were cultured in a mixed medium including Dulbecco's modified Eagle medium (DMEM) and Iscove's Modified Dulbecco's Medium (IMDM) with 10% fetal bovine serum (FBS) and 1% penicillin G-streptomycin on irradiated Mouse Embryonic Fibroblast (MEFs) feeder cells. *Eμ-myc/Arf–/–* and *Eμ-myc/p53–/–* cells were obtained from Dr. Scott Lowe's Laboratory (Cold Spring Harbor) in 2009. These cell lines were authenticated, showing that the *Arf* and *p53* genes were deleted, respectively, and that these murine cells overexpress the myc gene. PCR was used for detection with a specific primer. In 2010, we confirmed that the *Arf–/–* gene is deleted using PCR. Also in 2010 we confirmed that either Arf or p53 was deleted in the respective cell lines via western blotting.

Lentiviral Reporter Gene Construct

Firefly Luciferase (Luc2)-eGFP (LG), linked by "gcctctgctgcctctgcc" which encodes 6 amino acids (VSAVSA), was kindly provided by Dr. Christopher Contag (Stanford University). This vector contains the Ubiquitin C promoter sequence. The details can be found in Supplementary methods.

Murine Lymphoma Model

C57BL/6 mice were purchased from Charles River Laboratories (Wilmington, Massachusetts). All animal studies were approved by The Stanford University Institutional Animal Care and Use Committee. 1×10^6 EL-Arf–/– Lymphoma cells were diluted with 200 μl of PBS and injected intravenously via the tail vein as described (2). Control mice were injected with 200 μl of PBS.

Internal Window Chamber Implantation

Animals were anesthetized with isoflurane, hair was removed from mice using hair clippers and depilatory cream. An incision was made on the peritoneal skin and the left ILN was located on the internal side of the mouse skin by reference to the intersection of three large blood vessels on the interior after the tissue has been opened (see Figs. 1c). From the interior, our custom-made titanium frames were placed onto the ILN region and fixed in place using surgical sutures (Blue Polypropylene, 5-0, FS-2) (Med Rep Express, Patricia Brafford, MA). Thus this window chamber resides within the living animal with tissues above and surrounding it in this novel strategy. The skin was closed with surgical staples (Braintree Scientific, Inc., Braintree, MA). The details of the surgical procedure can be viewed online (Supplementary Movie 1).

Intravital microscopy

Images were collected with an intravital laser scanning microscope (IV-100, Olympus Corporation, Tokyo, Japan) using Olympus UplanFL objectives and Olympus FluoView FV300 version 4.3 software. ImageJ (NIH) and Olympus software was employed for image processing. Regions of the lymph nodes were excited with a set of lasers at 488 and 748 nm to detect EL-Arf–/– lymphoma cells and outline the blood vessels. The details can be found in Supplementary methods.

Bioluminescence Imaging

For bioluminescence imaging, 0.2 ml of 15 mg/ml D-Luciferin (Biosynth AG, Switzerland) was injected intraperitoneally into C57BL/6 mice under 1-2% inhaled isoflurane anesthesia. Bioluminescence signal was monitored using the IVIS system 200 series (Xenogen, Alameda, CA, USA), consisting of a highly-sensitive, cooled CCD camera. Living Image software (Xenogen, Alameda, CA, USA) was used to grid the imaging data and integrate the total bioluminescence signal in each region-of-interest (ROI). All bioluminescence images

were acquired with a 1 s exposure. Data were analyzed using total photon flux emission (photons/second) in the ROIs. Data was normalized using the background signal.

Analysis of EGFP positive cells

To assess EGFP+ cells in murine tissues, the BM, ILN, and spleen were isolated from C57BL/6 mice on day 7 and 14 after EL-Arf−/− cell inoculation. All tissues were minced and filtered with a 100 μm cell strainer (BD Falcon, Bedford, MA). The cells were analyzed by a FACScan flow cytometer (Becton Dickinson, San Jose, CA, USA).

Statistical analysis

Results were expressed as mean ± standard error of the mean. An unpaired, 2-tailed Student's t test was used to calculate P-values (except for Fig. 2d, in which a Wilcoxon test was employed). P-values of 0.05 or less were considered statistically significant.

Results

Eμ-myc Arf−/− Lymphoma Mouse Model

In order to image and analyze lymphoma development in detail, we applied a multimodal intravital fluorescence and bioluminescence imaging approach to an established lymphoma model(2)by transfecting a lentiviral vector containing firefly luciferase and EGFP sequences into the parental (*Eμ-myc Arf−/−* cells) line to generate EGFP/luc2 ("EL-Arf−/−") cells. To ensure that expression of firefly luciferase and EGFP protein does not induce abnormal biological function, we compared the cell growth patterns and the apoptosis sensitivity between the parental (*Eμ-myc Arf−/−* cells) and the lentivirus-transfected lymphoma cells (EL-Arf−/− cells). We confirmed there is no significant difference in cell growth and apoptosis sensitivity between the two sets of cells (Supplementary Fig. S1), which indicates that the reporter genes we inserted do not modify these lymphoma cell properties; furthermore, our results are consistent with results generated from the parental cell line(2, 22).

Previous studies on this lymphoma model have not elucidated tumor and angiogenesis development in the ILN. In initial experiments, we analyzed tumor development patterns using isosulfan blue to localize the lymph node and analyzed angiogenesis development using IVM. With IVM, we identified that microvascular number and circulating dye intensity was significantly higher in EL-Arf−/− lymphoma cell injected-mice compared to control mice from day 14 onward (Supplementary Fig. S2). Using macroscopic observation, we observed significant tumor development after day 14 compared with PBS-injected control mice (p<0.05) (Fig. 1 b-c).

In the Early Stage EL-Arf−/− Lymphoma Cells Expand in the Bone marrow (BM) and Spleen but not ILN

In order to understand cell proliferation patterns in mice at the whole-body level, we performed frequent (daily) bioluminescence imaging on living mice (N=12 per group) after injection of either EL-Arf−/− cells or PBS. On day 7 (and earlier), we detected bioluminescence signal in the BM and spleen but not in the ILN (Fig. 2a). We performed further analysis to validate our imaging results: we isolated the BM, ILN, and spleen from mice 7 days after EL-Arf−/− lymphoma cell- or PBS-injection, then the EGFP+ cell population was analyzed using flow cytometry. We detected a significant number of EGFP+ cells in the BM and spleen, but not in the ILN (Fig.2 b-c). PCR data also showed that less than 100 EL-Arf−/− lymphoma cells (if any) are located in the ILN by day 3 (Fig. 2d). Furthermore, we confirmed these results using *ex vivo* bioluminescence analysis on days 7 and 14 (Supplementary Fig. S3). These data collectively indicate that EL-Arf−/− cells

proliferated in both the BM and the spleen, but not in the ILN in the early stage of cancer progression.

Efflux of EL-Arf−/− lymphoma cells from the BM and spleen to the periphery in the middle stage

In the early stage of lymphoma dissemination, frequent bioluminescence imaging displayed an increasing signal in the BM and spleen (i.e., proliferation of EL-Arf−/− cells) but not the ILN. Yet interestingly, toward the middle stage (after day 8), we observed decreased bioluminescence signal in the BM (66.5±8.7, day 8 vs. day 8.5) and spleen (36.0±3.6, day 8 vs. day 8.5) with a concomitant increase in signal in the ILN (215.0±57.0, day 8 vs. day 9) (N=12 EL-Arf−/− injected group, N=5 control mice) (Fig.3 a-b). The phenomenon observed is thus highly reproducible and the timepoint at which it occurs post-injection is rather specific. Moreover, when we increased the initial injection cell number five-fold (to 5×10^6 EL-Arf−/− cells), we reproducibly observed a much earlier efflux of EL-Arf−/− lymphoma cells around day 5 (Supplementary Fig. S4). This result may reveal a dependence of the efflux on local cell concentration. Furthermore, even when injecting EL-Arf−/− lymphoma cells directly into the spleen (rather than via tail vein, so that no cells could have initially seeded the periphery), importantly we observed the same phenomenon: efflux from spleen and influx to ILN (Supplementary Fig. S5). These results strongly indicate that EL-Arf−/− lymphoma cells proliferate in the spleen and BM, then flow out from these sites to the periphery. Importantly, we also observed the same efflux/influx phenomenon using a different lymphoma cell type (p53−/− crossed with *Eμ-myc* and transfected with EGFP/luc2, termed EL-p53−/−) via bioluminescence imaging (Supplementary Fig. S6).

Sudden, huge influx of the lymphoma cells into peripheral lymph node

In order to sequentially image the genesis of lymphoma in the ILN at the microscale, we developed a novel LNIWC. It consisted of a titanium frame (9.0 mm diameter, 2.0 mm thickness and 0.35 g). An incision was made on the peritoneal skin, and the ILN was located visually by the vascular pattern (Supplementary Movie 1). The LNIWC was then implanted over the ILN. The LNIWC was fixed in place with sutures and the peritoneal region was closed with surgical clips (Fig. 4a-c and Supplementary Movie 1). Surgical clips were removed and access to the window was obtained every time IVM was performed, then the clips were replaced each time. This approach enables us to serially obtain IVM images for up to two weeks, and we validated the technique's utility against two other methods for visualizing the ILN sequentially on the microscale (see Supplementary Table 1). These two other methods are similar to techniques which have been employed for imaging other abdominal organs such as liver and other "body windows," but they suffered from difficulties due primarily to the unique challenges of serially imaging the lymph node in living subjects (as a result of the intimate vascular connections between lymph node and adjacent tissue, these techniques suffered from tissue adhesions and fibrosis, see Supplementary Information). We chose to employ the LNIWC method in our experiments due to its ability to considerably decrease autofluorescence in serial imaging sessions and because it provided a fiduciary marker for us to consistently return to precisely the same sites to image them longitudinally (see Supplementary Information). We observed neither loss in body weight (p=0.67) nor any unusual mouse behavior throughout the observation period in both the LNIWC and non-LNIWC groups (Fig. 4e, Supplementary movie 2). We were also able to observe macroscopic tumor growth in the LNIWC (Fig. 4f). In accordance with our PCR and bioluminescence data, we were unable to detect EGFP-expressing cells in the inguinal lymph node until day 9±1 day after injection of the EL-Arf−/− cell group (N=7 mice) using IVM; on the other hand, we never detected EGFP signal from the control (PBS-injected) mice (N=4) (Fig. 5a-b) (Supplementary Fig. S7). We also observed the same reproducible phenomena in our other lymphoma model, the EL-p53−/− injected mice, using

IVM (Supplementary Fig. S8). Furthermore, using the LNIWC with IVM high-resolution imaging, we observed a single circulating EL-Arf−/− lymphoma cell in the vasculature feeding the ILN on day 10 (Supplementary Movie 3), while we never observed tumor cells in vasculature on other days. This suggests that effluxed lymphoma cells likely reach and seed the periphery via blood circulation. FACS and PCR analyses validated that no tumor cells were present in ILN both 3 days and 1 week after EL-Arf−/− injection (Fig. 2b-d). Because we were able to image the same mouse at the same site every 2-3 days, we observed a relatively sudden EL-Arf−/− cell influx into the ILN between day 8-10 post-injection. In order to focus on this time period, we obtained IVM-images every 12 hours from 8-10 days post-injection of cells. Intriguingly, we observed a sudden large influx of EL-Arf−/− cells into the ILN within a 12 h time period reproducibly across N=7 mice (Fig. 5b-c). Therefore, the LNIWC, which has not been previously described for intravital imaging, enabled us to visualize the ILN longitudinally and observe the "burst effect" of cells into the ILN.

Using immunohistochemistry we then showed that after these cells arrive, the EL-Arf−/− lymphoma cells establish a rapidly proliferating tumor in the ILN (Supplementary Fig. S9). These results together indicate that EL-Arf−/− lymphoma cells flow out from the spleen/BM to the periphery via the circulation in the middle stage and then proliferate to form a tumor in peripheral lymph nodes (including the ILN and superficial cervical lymph nodes, see Fig. 3). Further, these results suggest the spleen must be somehow conditioned for efflux and underscore the utility of multimodal IVM and bioluminescence imaging to visualize tumor cell trafficking in live mice.

Discussion

Malignant transformation of normal lymphocytes results in lymphoma, and many lymphoma subtypes migrate and disseminate. This dissemination may reflect conserved physiologic behavior unlike the metastasis of other cancers, considering that normal lymphocyte homing and recirculation molecules have been implicated in lymphoma dissemination and invasion. Since the time course and mechanisms of lymphoma trafficking are not well-understood, we developed a multimodal imaging platform to sequentially image lymphoma cells; we combined a novel LNIWC technique for IVM with bioluminescence imaging to derive time course and basic mechanistic information on lymphoma development.

The LNIWC, which represents a modification of previous window chamber techniques(23), was developed to obtain sequential images. The LNIWC method can be used to serially image (up to two weeks for 6-7 independent imaging sessions) the ILN to observe lymphoma progression in an orthotopic mouse lymphoma model under physiological conditions. Critically, the method also enabled us to easily find and image the same location during each imaging session because of the ability to use the LNIWC as a spatial point-of-reference, including suture holes and the chamber itself for spatial orientation. To our knowledge, this technique enables the first instance of serial imaging of a lymph node in a living mouse.

Using multimodal (intravital/bioluminescence) imaging, we discovered a key, novel feature of the EL-Arf−/− lymphoma model: tumor cell initiation and expansion in the bone marrow and spleen, followed by a burst into peripheral lymph nodes and progression in the ILN. It is notable that this cell line is not unique in this respect - we observed that the EL-p53−/− cell line also displayed a similar, reproducible pattern of efflux/influx (Supplementary Figs. S6 and S8), suggesting the mechanism we observed is not model-dependent and is likely to be a more general feature of lymphoma dissemination. The insights achieved with these models could prove invaluable in understanding how different genetic alterations can influence

migration of lymphoid cells to different lymphoid sites as these models are in many ways similar to human lymphoma (2, 3).

We note that prior to this work, the lymph node tumors in these murine models were evaluated primarily via palpation and whole-body fluorescence imaging, which are not sensitive to low numbers of tumor cells and thus do not provide detailed information particularly at the earlier time points. Therefore, it was previously presumed that in the *Eμ-myc* lymphoma model tumors began forming within the lymph node immediately after the intravenous injection of cells(2). Given the previous assumptions, we were initially surprised to find a lack of lymphoma cells in the ILN during the first ~9 days after injection using IVM. Our findings using the LNIWC, which were further validated by bioluminescence, FACS, and PCR analyses, collectively demonstrate that around day 9 tumor cells exit the spleen and BM and at least some fraction of these cells very reproducibly and robustly reach the ILN. It was surprising to us that lymphoma cells do not gradually depart from the spleen and BM into the ILN, but instead they arrive rapidly in a burst into the ILN. While the murine lymphoma model differs in several aspects from human lymphoma, our pre-clinical findings do mirror distribution patterns in human lymphoma such as splenic marginal zone lymphoma (SMZL) and chronic lymphocytic leukemia (CLL) in the later stages. Early in these diseases, lymphoma cells appear in the bone marrow and spleen, without significant peripheral node involvement. In later stages, lymphoma cells can often be found in other organs(24-27) with increasing tumor burden and even after successful treatment, lymphoma cells may "re-seed" the original lymph nodes/lymphoma(28). This re-seeding can critically accelerate tumor growth, angiogenesis, and the recruitment of stromal elements(28). Our model may be applicable to these and other Non-Hodgkin's and Hodgkin's Lymphomas, where the BM and spleen could serve as reservoirs for cells that seed and re-seed recurrent sites of disease. Understanding the pattern and mechanisms of lymphoma progression could unlock new ways to detect and treat this disease. More generally, our model may help answer key questions about the interplay of host factors and microenvironment that allow malignant cells to home to, proliferate at, and exit from specific sites of disease in a wide range of hematologic and solid tumors. Therefore, with the advent of biologic therapies and immune modulation for treatment of cancer, understanding what triggers this efflux, and critically finding ways to delay or even stop it, may enable physicians to interfere with disease spreading, re-seeding, or further metastasizing.

In conclusion, our multimodal intravital (LNIWC) and bioluminescence approach enabled us to explore how a lymphoma mass truly evolves within the lymph node; this led us to discover lymphoma cell efflux from the spleen and BM and a concomitant influx into the ILN within a surprisingly short time period. This finding has implications for understanding and developing novel treatment regimens for human lymphoma and potentially other cancers.

Supplementary Material

Refer to Web version on PubMed Central for supplementary material.

Acknowledgments

References

1. Lenz G, Staudt LM. Aggressive lymphomas. N Engl J Med. 2010; 362:1417–29. [PubMed: 20393178]

2. Schmitt CA, Fridman JS, Yang M, Lee S, Baranov E, Hoffman RM, et al. A senescence program controlled by p53 and p16INK4a contributes to the outcome of cancer therapy. Cell. 2002; 109:335–46. [PubMed: 12015983]

3. Lowe SW, Sherr CJ. Tumor suppression by Ink4a-Arf: progress and puzzles. Curr Opin Genet Dev. 2003; 13:77–83. [PubMed: 12573439]

4. Swirski FK, Nahrendorf M, Etzrodt M, Wildgruber M, Cortez-Retamozo V, Panizzi P, et al. Identification of splenic reservoir monocytes and their deployment to inflammatory sites. Science. 2009; 325:612–6. [PubMed: 19644120]

5. Deguine J, Breart B, Lemaitre F, Di Santo JP, Bousso P. Intravital imaging reveals distinct dynamics for natural killer and CD8(+) T cells during tumor regression. Immunity. 2010; 33:632–44. [PubMed: 20951068]

6. Mempel TR, Pittet MJ, Khazaie K, Weninger W, Weissleder R, von Boehmer H, et al. Regulatory T cells reversibly suppress cytotoxic T cell function independent of effector differentiation. Immunity. 2006; 25:129–41. [PubMed: 16860762]

7. Yang M, Jiang P, Hoffman RM. Whole-body subcellular multicolor imaging of tumor-host interaction and drug response in real time. Cancer Res. 2007; 67:5195–200. [PubMed: 17545599]

8. Yang M, Baranov E, Wang JW, Jiang P, Wang X, Sun FX, et al. Direct external imaging of nascent cancer, tumor progression, angiogenesis, and metastasis on internal organs in the fluorescent orthotopic model. Proc Natl Acad Sci U S A. 2002; 99:3824–9. [PubMed: 11891294]

9. Kedrin D, Gligorijevic B, Wyckoff J, Verkhusha VV, Condeelis J, Segall JE, et al. Intravital imaging of metastatic behavior through a mammary imaging window. Nature methods. 2008; 5:1019–21. [PubMed: 18997781]

10. Fukumura D, Duda DG, Munn LL, Jain RK. Tumor microvasculature and microenvironment: novel insights through intravital imaging in pre-clinical models. Microcirculation. 2010; 17:206–25. [PubMed: 20374484]

11. Lohela M, Werb Z. Intravital imaging of stromal cell dynamics in tumors. Current opinion in genetics & development. 2010; 20:72–8. [PubMed: 19942428]

12. Smith BR, Cheng Z, De A, Koh AL, Sinclair R, Gambhir SS. Real-time intravital imaging of RGD-quantum dot binding to luminal endothelium in mouse tumor neovasculature. Nano Lett. 2008; 8:2599–606. [PubMed: 18386933]

13. Smith BR, Cheng Z, De A, Rosenberg J, Gambhir SS. Dynamic visualization of RGD-quantum dot binding to tumor neovasculature and extravasation in multiple living mouse models using intravital microscopy. Small. 2010; 6:2222–9. [PubMed: 20862677]

14. Smith BR, Kempen P, Bouley D, Xu A, Liu Z, Melosh N, et al. Shape Matters: Intravital Microscopy Reveals Surprising Geometrical Dependence for Nanoparticles in Tumor Models of Extravasation. Nano letters. 2012; 12:3369–77. [PubMed: 22650417]

15. Miyazaki J, Tsuzuki Y, Matsuzaki K, Hokari R, Okada Y, Kawaguchi A, et al. Combination therapy with tumor-lysate pulsed dendritic cells and antiangiogenic drug TNP-470 for mouse pancreatic cancer. Int J Cancer. 2005; 117:499–505. [PubMed: 15906361]

16. Arad A, Proulle V, Furie RA, Furie BC, Furie B. {beta}2 glycoprotein-1 autoantibodies from patients with antiphospholipid syndrome are sufficient to potentiate arterial thrombus formation in a mouse model. Blood. 2011; 117:3453–9. [PubMed: 21245481]

17. von Andrian UH. Intravital microscopy of the peripheral lymph node microcirculation in mice. Microcirculation. 1996; 3:287–300. [PubMed: 8930886]

18. Diacovo TG, Puri KD, Warnock RA, Springer TA, von Andrian UH. Platelet-mediated lymphocyte delivery to high endothelial venules. Science. 1996; 273:252–5. [PubMed: 8662511]

19. Gowans JL. Life-span, recirculation, and transformation of lymphocytes. Int Rev Exp Pathol. 1966; 5:1–24. [PubMed: 4877345]

20. Gallatin M, St John TP, Siegelman M, Reichert R, Butcher EC, Weissman IL. Lymphocyte homing receptors. Cell. 1986; 44:673–80. [PubMed: 3004743]

21. Pals ST, de Gorter DJ, Spaargaren M. Lymphoma dissemination: the other face of lymphocyte homing. Blood. 2007; 110:3102–11. [PubMed: 17656647]

22. Schmitt CA, McCurrach ME, de Stanchina E, Wallace-Brodeur RR, Lowe SW. INK4a/ARF mutations accelerate lymphomagenesis and promote chemoresistance by disabling p53. Genes Dev. 1999; 13:2670–7. [PubMed: 10541553]

23. Bertera S, Geng X, Tawadrous Z, Bottino R, Balamurugan AN, Rudert WA, et al. Body window-enabled in vivo multicolor imaging of transplanted mouse islets expressing an insulin-Timer fusion protein. Biotechniques. 2003; 35:718–22. [PubMed: 14579736]

24. Matutes E, Oscier D, Montalban C, Berger F, Callet-Bauchu E, Dogan A, et al. Splenic marginal zone lymphoma proposals for a revision of diagnostic, staging and therapeutic criteria. Leukemia. 2008; 22:487–95. [PubMed: 18094718]

25. Mazloom A, Rodriguez A, Ha CS, Medeiros LJ, Wogan C, Shihadeh F, et al. Incidence of gastric involvement in patients with nongastrointestinal extranodal marginal zone lymphoma. Cancer. 2011; 117:2461–6.

26. Mollejo M, Lloret E, Menarguez J, Piris MA, Isaacson PG. Lymph node involvement by splenic marginal zone lymphoma: morphological and immunohistochemical features. Am J Surg Pathol. 1997; 21:772–80. [PubMed: 9236833]

27. Ghia P, Ferreri AM, Caligaris-Cappio F. Chronic lymphocytic leukemia. Crit Rev Oncol Hematol. 2007; 64:234–46. [PubMed: 17544290]

28. Kim MY, Oskarsson T, Acharyya S, Nguyen DX, Zhang XH, Norton L, et al. Tumor self-seeding by circulating cancer cells. Cell. 2009; 139:1315–26. [PubMed: 20064377]
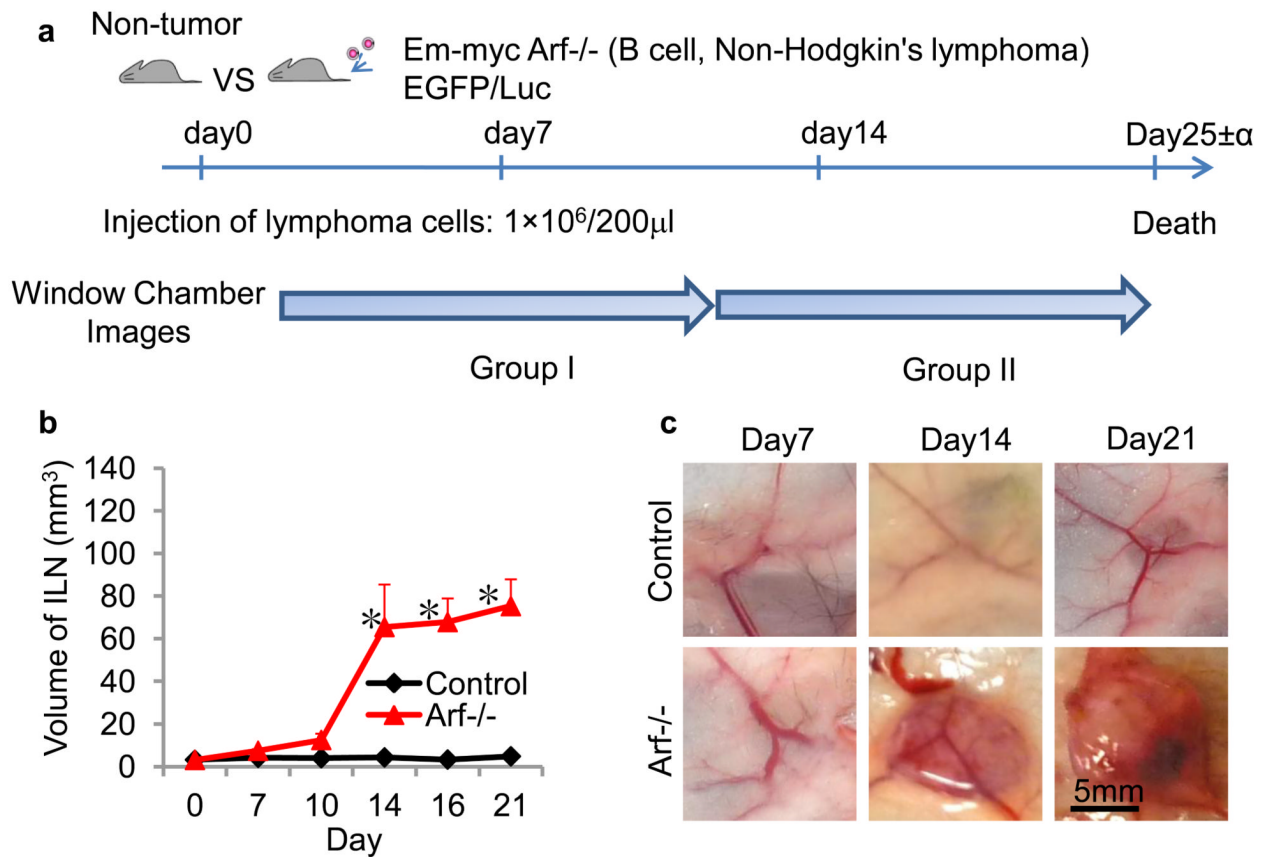
a Non-tumor VS Eµ-myc Arf-/- (B cell, Non-Hodgkin's lymphoma) EGFP/Luc

day0 — day7 — day14 — Day25±α

Injection of lymphoma cells: 1×10^6/200µl

Death

Window Chamber Images

Group I Group II

b

c Day7 Day14 Day21

Control

Arf-/-

5mm

Figure 1. Mouse lymphoma model

a) EL-Arf–/– cells (1×10^6) were tail-vein injected into C57BL/6 mice. LNIWC imaging was separated into 2 groups: group I was focused upon from day 0 through day 10, and for group II from day 11 through day 17. This was done because of the limitation of repeatedly opening the staples up to 6-7 times in the same mouse. N=7 mice were imaged with IVM in each group in six independent experiments. b) Tumor development in the ILN. Symbols represent the means of ILN volumes determined by N=3-7 animals for each point. Bars: S.E.M. *p < 0.05. c) Representative images of the ILN on Days 7, 14, and 21 post-injection.
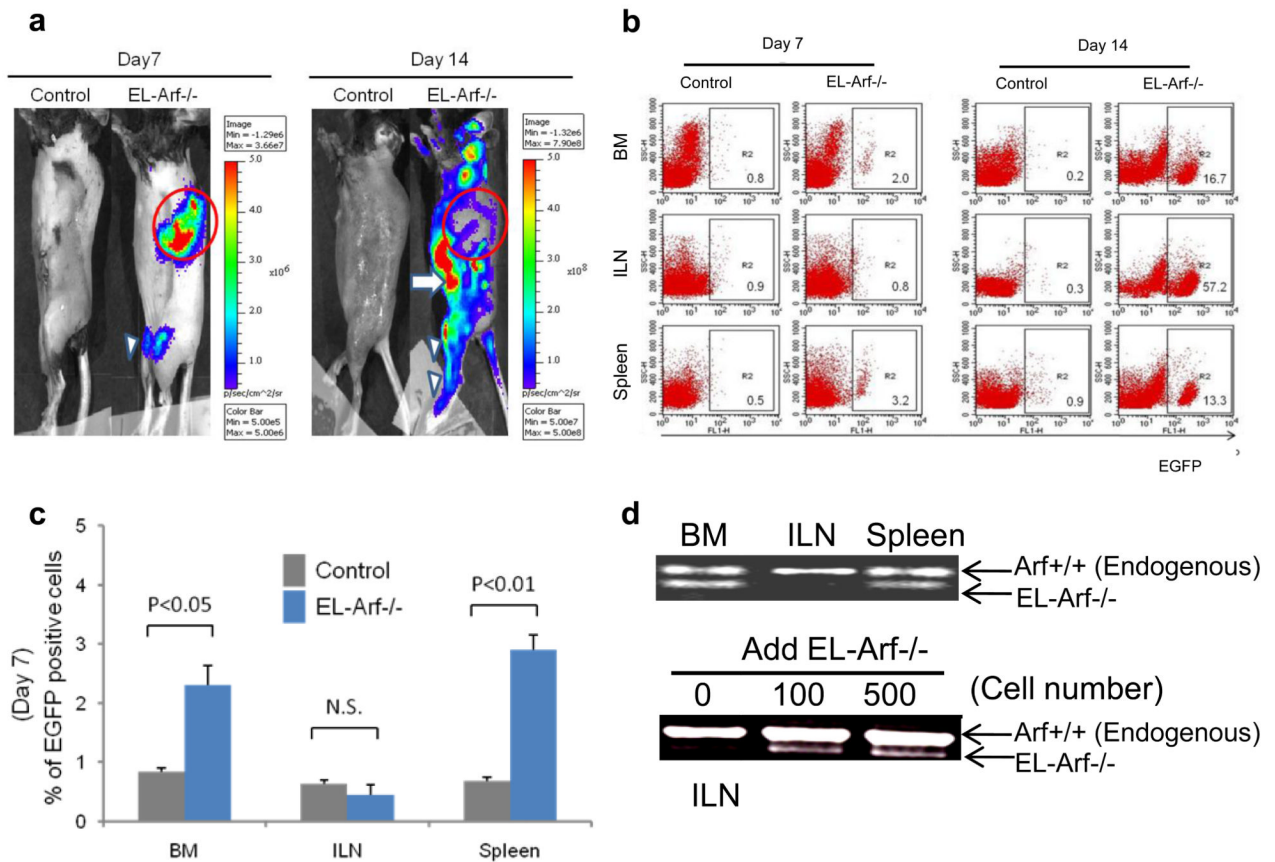
Figure 2. Lymphoma cells proliferate in the Bone marrow (BM) and Spleen but not in the ILN node in the early stage

Bioluminescence images were acquired after injection of EL-Arf−/− cells or control. a) Bioluminescence images are shown on day 7 and 14. The arrow designates the ILN, which is visible with bioluminescence by day 14. The arrowhead shows bone marrow (femur) and the red circleindicates spleen (N=10 each group). b) and c) EGFP+ cell analysis using FACS. b) Representative FACS dot plot of EGFP+ cells in BM, spleen, and ILN on day 7 and 14 after injection. c) The columns represent the means of percentages of EGFP+ cells from three independent experiments (N=8 each group). Bars, S.E.M. *p<0.05 d) Expression analysis of EL-Arf−/− lymphoma cells in mouse inguinal lymph node using highly-sensitive PCR on day 3. The upper panel shows either Arf+/+ (endogenous normal cells) or EL-Arf−/− lymphoma cell expression pattern. The lower panel shows quantitative PCR. The indicated EL-Arf−/− cell number was exogenously added into the ILN directly, demonstrating that while we can detect as few as 100 EL-Arf−/− cells in the ILN, no lymphoma cells are detectable in an EL-Arf−/− injected mouse on day 3 (N=3, performed over three independent experiments).
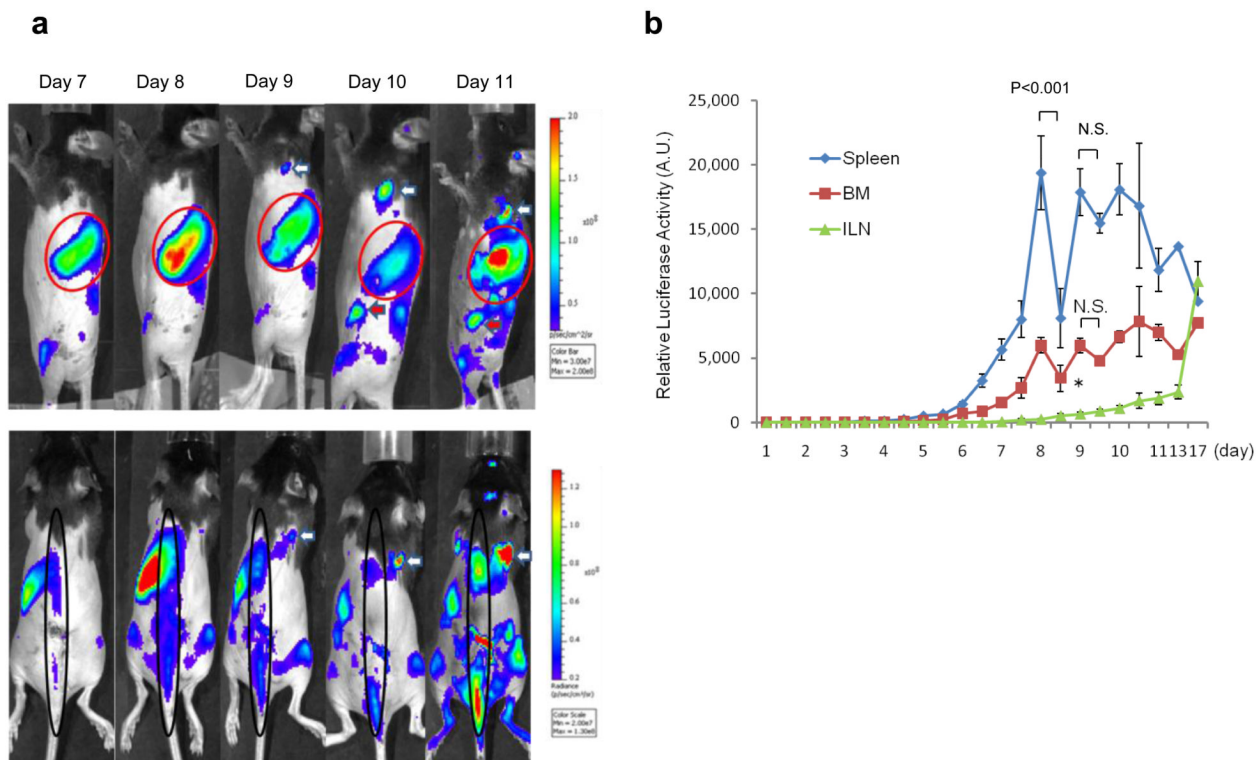
Figure 3. Efflux of lymphoma cells from the spleen and Bone Marrow (BM) to the periphery in the middle stage

a) Representative bioluminescence images (from N=12 mice) in an EL-Arf−/− cell injected mouse. The top panel shows mice placed on their side; the red arrow indicates the ILN and the white arrow indicates a superficial cervical lymph node. The red circle designates the spleen. The bottom panel displays prone images; the black circle designates the bone marrow and the white arrow indicates a superficial cervical lymph node. b) Average bioluminescence signal from the BM, ILN and spleen over time. Each point represents the bioluminescence signal from seven to twelve mice in four independent experiments. * indicates P<0.05. Bars, S.E.M.
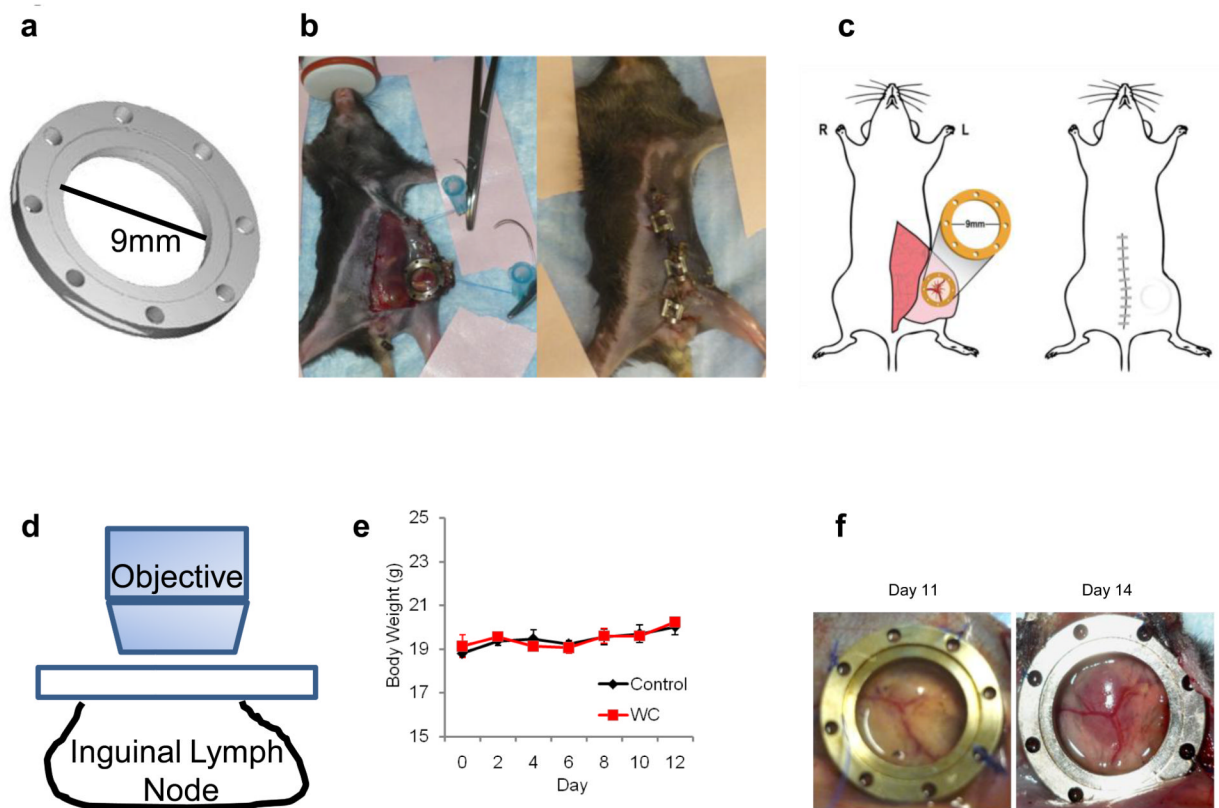
Figure 4. Development of the lymph node window chamber technique

a) Schematic of the titanium lymph node window chamber. b) Representative picture of a mouse after implantation of the LNIWC over the mouse ILN (left). The surgical clips are used to close the skin until the next imaging session (right). c) Schematic of the placement of the LNIWC after surgical implantation (left) over the ILN, and a schematic of the mouse after closing the skin using surgical clips (right). d) Schematic of IVM being performed using the LNIWC. e) Body weight measurements of C57BL/6 mice either carrying the LNIWC (WC) or not (control). Symbols represent the means of body weight. N=3 mice per group in a single independent experiment. Bars: S.E.M. f) Representative pictures of tumor growth in the LNIWC.
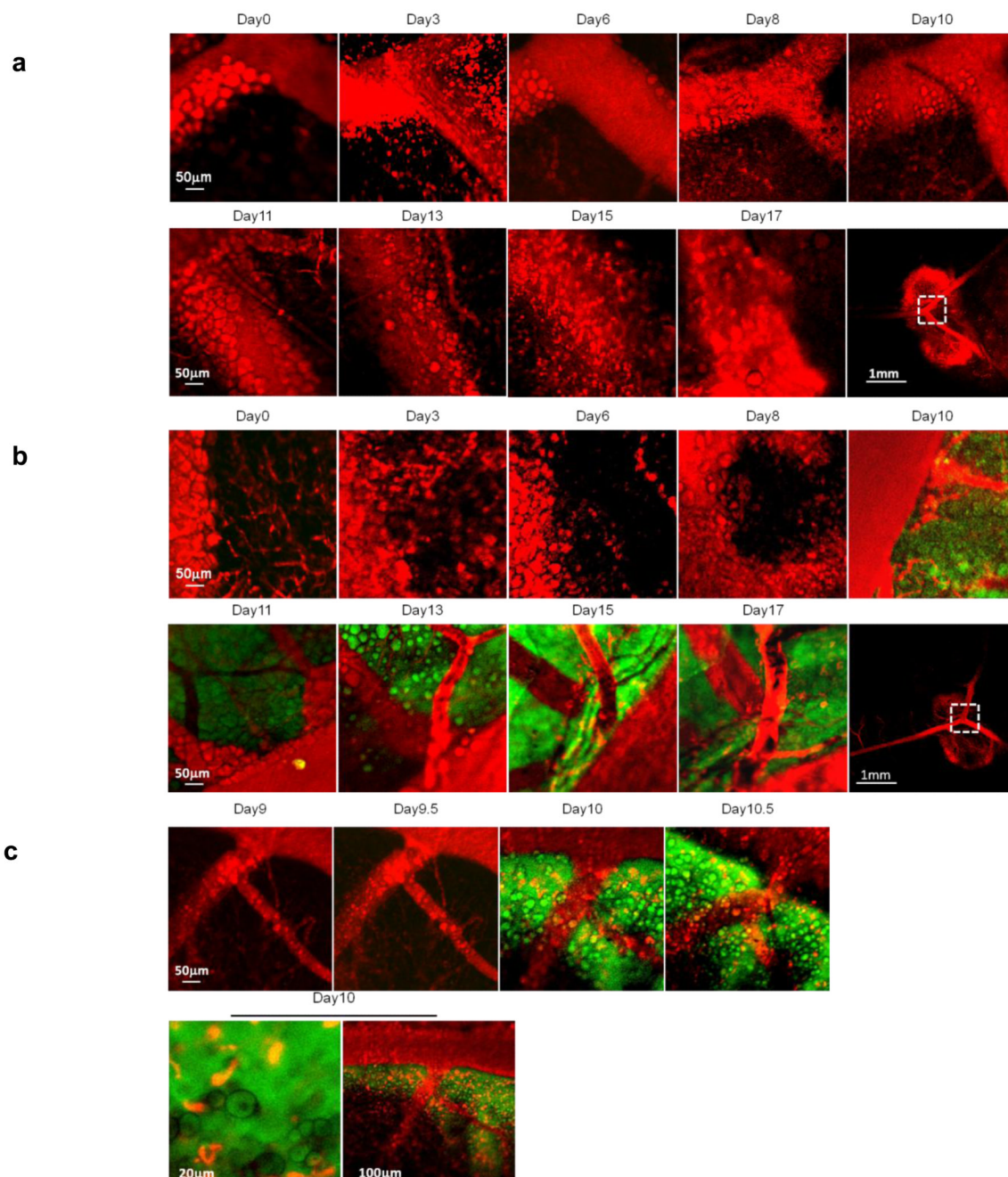
Figure 5. Lymph node internal window chamber images
a) Control mouse images from Day 0 through Day 17. The final panel represents the larger-scaleregion that was imaged. b) IVM imaging of EL-Arf−/− cell-injected mice. c) High temporal resolution images obtained twice daily of EL-Arf−/− cell-injected mice. Red: blood vessels (via dye) and adipocytes (by autofluorescence). Green: EL-Arf−/− cells. Yellow: indicates merged green/red regions. We validated these data in N=7 mice per group, with the experiment performed independently six times.